Translational Oncology
www.transonc.com

Volume 11 Number 5 October 2018 pp. 1232–1243 1232

Establishment and Characterization of Paired Primary and Peritoneal Seeding Human Colorectal Cancer Cell Lines: Identification of Genes That Mediate Metastatic Potential[1]

Soon-Chan Kim[*,†,2], Chang-Won Hong[‡,2], Sang-Geun Jang[*], Ye-Ah Kim[*], Byong-Chul Yoo[‡], Young-Kyoung Shin[*], Seung-Yong Jeong[*,§], Ja-Lok Ku[*,†] and Jae-Gahb Park[*,§]

[*]Korean Cell Line Bank, Laboratory of Cell Biology, Cancer Research Institute, Seoul National University College of Medicine, Seoul 03080, Korea; [†]Department of Biomedical Sciences, Seoul National University College of Medicine, Seoul 03080, Korea; [‡]Colorectal Cancer Branch, Research Institute, National Cancer Center, 323 Ilsan-ro, Ilsandong-gu, Goyang-si, Gyeonggi-do 10408, Korea; [§]Department of Surgery, Seoul National University College of Medicine, 101 Daehak-ro, Yeongeon-dong, Jongno-gu, Seoul 03080, Korea

Abstract

Peritoneal metastasis is one of the major patterns of unresectability in colorectal cancer (CRC) and a cause of death in advanced CRC. Identification of distinct gene expressions between primary CRC and peritoneal seeding metastasis is to predict the metastatic potential of primary human CRC. Three pairs of primary CRC (SNU-2335A, SNU-2404A, and SNU-2414A) and corresponding peritoneal seeding (SNU-2335D, SNU-2404B, and SNU-2414B) cell lines were established to determine the different gene expressions and resulting aberrated signaling pathways in peritoneal metastasis tumor using whole exome sequencing and microarray. Whole exome sequencing detected that mutation in *CYP2A7* was exclusively shared in peritoneal seeding cell lines. Microarray identified that there were five upregulated genes (*CNN3*, *SORBS1*, *BST2*, *EPSTI1*, and *KLHL5*) and two downregulated genes (*TRY6* and *STYL5*) in the peritoneal metastatic cell lines. *CNN3* expression was highly augmented in both mRNA and protein levels in peritoneal metastasis cells. Knockdown of Calponin 3 resulted in augmented level of E-cadherin in peritoneal metastasis cells, and migration and invasiveness decreased accordingly. We suggest that *CNN3* takes part in cell projection and movement, and the detection and distribution of *CNN3* may render prognostic information for predicting peritoneal seeding metastasis from primary colorectal cancer.

Translational Oncology (2018) 11, 1232–1243

Introduction

Colorectal cancer (CRC) is the second most common cause of cancer-related deaths in developed countries. In Korea, CRC incidents are increasing annually as the third most common cancer [1]. Peritoneal metastasis is one of the major patterns of unresectability in CRC and a cause of death in advanced CRC. In spite of improvements in chemotherapy and surgical techniques, prognoses for peritoneal metastasis remain unfavorable [2]. Peritoneal carcinomatosis is considered as a sequence of events that together form a peritoneal metastatic cascade. Initial exfoliation of malignant cells is reported to involve several adhesion molecules, including E-cadherin, CD44, Selectins, and various leukocyte-associated antigens [3,4]. Intraperitoneal tumor dissemination is partly promoted by tumor-induced

Address all correspondence to: Ja-Lok Ku or Jae-Gahb Park, Korean Cell Line Bank, Laboratory of Cell Biology, Cancer Research Institute, Seoul National University College of Medicine, Seoul 03080, Korea.
E-mail: kujalok@snu.ac.kr, jgpark88@gmail.com

[1] Funding: This study was funded in part by the Korean Cell Line Research Foundation and the Priority Research Center Program (2009-0093820) through a National Research Foundation of Korea grant funded by the MSIP. The first author received a scholarship from the BK21-plus education program provided by the National Research Foundation of Korea.
[2] These authors contributed equally to this work.
Received 8 May 2018; Accepted 23 July 2018

1936-5233/18
https://doi.org/10.1016/j.tranon.2018.07.014

mesothelial apoptosis mediated via Fas/FasL mechanism [5]. Attachment to the submesothelial tissue is mainly mediated by adhesion molecules such as ICAM-1, PECAM-1, and VCAM-1, which are expressed by mesothelial cells. Integrin also plays important role in adhesion to the basement membrane [6,7]. Invasion into the subperitoneal space is induced by HGF/SF produced by mesothelial cells. Subsequent infiltration of the peritoneal-blood barrier occurs via degradation by proteases [8]. Recent genomic profiling studies have identified distinct gene expression patterns, determining CRC spreading to the liver, the peritoneum, or both. For instance, Diep et al. profiled that peritoneal carcinomatoses and liver metastases tend to have more DNA copy number changes than original lesions [9]. Kleivi et al. reported that chromosome arm 5p gains are common in peritoneal carcinomatoses, and 20 genes (including PTGER4, SKP2, and ZNF622) mapping in this region were overexpressed in the tumors [10]. Nevertheless, the complexity of peritoneal metastatic cascade and molecular cross talk between tumor cells and host elements demands for the development of new therapeutic targets for peritoneal seeding [11]. Thus, establishing peritoneal metastatic cell lines and identifying distinct gene expression patterns in the peritoneal seeding compared to the matched primary CRC will improve our understanding of the mechanisms responsible for peritoneal seeding metastases [9,10].

In this paper, three pairs of primary CRC and corresponding peritoneal seeding cell lines were established and analyzed by the whole exome sequencing and microarray to identify distinct mutational statuses and gene expressions between primary CRC and peritoneal seeding metastasis.

Methods

Cell Line Establishment

Cell lines were established from pathologically proven colorectal carcinomas. Detailed procedure was described previously [12]. The locations and stages of original tumors were listed in Table 1.

DNA Fingerprinting Analysis

The genomic DNA from each cell line was amplified using the AmpFlSTR identifiler PCR amplification kit (Applied Biosystems, Foster City, CA). Detailed procedure was described previously [12]. The STR profiles of established peritoneal metastasis cancer cell lines and their parental colorectal cancer cell lines are listed in supplementary Table 23.

Cell Growth Properties

Suspensions of 5×10^4 cells were added to 35-mm tissue culture dishes containing culture medium. The number of cells was counted in triplicate at 24-hour intervals for at least 10 days. The doubling time of the cells was calculated from the growth phase. Cell viability was determined with 0.4% trypan blue dye, and the number of viable cells was counted using countess automated cell counter (Invitrogen, Carlsbad,CA). The morphology of cells grown in T-75-cm^2 culture flasks was observed daily by phase-contrast microscopy. In addition, mycoplasma contamination was tested by the 16S-rRNA gene-based PCR amplification method using the e-Myco Mycoplasma PCR detection kit (Intron Biotechnology, Gyeonggi, Korea).

Cell Cultures

Forty-eight human CRC cell lines (SNU-61, SNU-70, SNU-81, SNU-175, SNU-254, SNU-283, SNU-407, SNU-479, SNU-503, SNU-769A, SNU-769B, SNU-796, SNU-977, SNU-1033, SNU-1040, SNU-1047, SNU-1181, SNU-1197A, SNU-1235, SNU-1411, SNU-1406, SNU-1544, SNU-1684, SNU-1746, SNU-C1, SNU-C2A, SNU-C4, SNU-C5, Caco-2, COLO201, COLO205, COLO320, DLD1, HCT-8, HCT-15, HCT-116, HT-29, LoVo, LS174T, NCI-H716, SW-403, SW-480, SW-620, SW-1116, WiDr, KM12C, KM12SM, and KM12L4) were obtained from the Korean Cell Line Bank. All cell lines were maintained in RPMI1640 media with 10% fetal bovine serum at 37°C and 5% CO_2. All cell lines were tested and authenticated by Korean Cell Line Bank using DNA finger printing analysis.

Nucleic Acid Isolation and Complementary DNA Synthesis

Genomic DNA was extracted from the cell lines using QIAamp DNA Mini Kit (Qiagen, Hilden, Germany), and RNA was extracted using the TRIzol (Life Technologies, Carlsbad, CA) and RNeasy Plus Mini Kit (Qiagen) according to manufacturer's protocol. For cDNA synthesis, QuantiTect Reverse Transcription Kit (Qiagen) was used. One microgram of total RNA, 2 μl of gDNA Wipeout Buffer, and DEPC water up to 14 μl were mixed together and incubated at 42°C for 2 minutes. The mixture was mixed with Quantiscript RT Buffer, RT Primer Mix, and Quantiscript Reverse Transcriptase and incubated at 42°C for 45 minutes. Finally, the mixture was incubated at 95°C for 2 minutes and cooled down to room temperature.

Microarray Analyses

Total RNA was extracted using TRIzol (Life Technologies, Carlsbad, CA) and purified with the RNeasy Mini Kit (Qiagen, Hilden, Germany). RNA integrity was assessed with an Agilent 2100 Bioanalyzer (Agilent, Palo Alto, CA). High-quality RNA (RNA integrity number > 9.0) was used for the gene expression microarray analysis (Affymetrix, Inc., Santa Clara, CA). After 16 hours of

Table 1. Clinicopathologic Characteristics of Three Paired Colon Cancer Cell Lines

	In Vitro					*In Vivo*			
	Growth Pattern	Doubling Time (h)	Cell Morphology	Sex	Age	Original Site of Cell Line	Pathology	TNM Stage	MSI Status
SNU-2335A	Adherent	45	Stellate	F	55	Sigmoid colon mass	M/D Adenocarcinoma	T3N2M1	MSS
SNU-2335D	Adherent	48	Polygonal	F	55	Omental seeding nodule		T3N2M1	MSS
SNU-2335E	Adherent	40	Polygonal	F	55	Krukenberg tumor mass		T3N2M1	MSS
SNU-2404A	Adherent	55	Polygonal	F	62	Ascending colon mass	M/D Adenocarcinoma	T4bN2M1	MSS
SNU-2404B	Adherent/ floating	67	Round/Polygonal	F	62	Omental seeding nodule		T4bN2M1	MSS
SNU-2414A	Adherent	45	Polygonal	M	76	Sigmoid colon mass	P/D Adenocarcinoma	T4bN2M1	MSS
SNU-2414B	Adherent	29	Polygonal	M	76	Omental seeding nodule		T4bN2M1	MSS

M/D, moderately differentiated; *P/D*, poorly differentiated; MSS, microsatellite stable.

hybridization at 45°C, the arrays were washed and stained on a GeneChip Fluidics Station (Affymetrix, Inc.) and scanned using the Gene Chip Scanner 3000 (Affymetrix, Inc.). The CEL intensity data extracted by GCOS (Gene Chip Operating Software) and Affymetrix Expression Console software with the default RMA parameters were used for data analysis.

Whole Exome Sequencing

SureSelect sequencing libraries were prepared according to manufacturer's instructions (Agilent sureselect all Exon kit 50 Mb) using the Bravo automated liquid handler. Three micrograms of genomic DNA was fragmented to a median size of 150 bp using the Covaris-S2 instrument (Covaris, Woburn, MA). The adapter ligated DNA was amplified by PCR, and the PCR product quality was assessed by capillary electrophoresis (Bioanalyzer, Agilent). The hybridization buffer and DNA blocker mix were incubated for 5 minute at 95°C and then for 10 minutes at 65°C in a thermal cycler. The hybridization mixture was added to the bead suspension and incubated for 30 minutes at RT while mixing. The beads were washed, and DNA was eluted with 50 ml SureSelect elution buffer (Agilent). The flow cell loaded on HISEQ 2500 sequencing system (Illumina).

qRT-PCR

Detailed procedure was described previously [12]. The primers that were used in this study are listed in supplementary table 21.

Protein Isolation and Western Blotting

Cells were harvested with a cell scraper after washing with cold PBS. Whole protein was extracted with EzRIPA buffer (ATTO Co., Tokyo, JAPAN) supplied with 1% protease inhibitor and 1% of phosphatase inhibitor. The protein concentration was calculated by SMART micro BCA protein assay kit (Intron Biotechnology, Gyeonggi, Korea). Equal amounts of protein were loaded on 4%-15% Mini-PROTEAN TGX Precast Gels (BIO-RAD, Hercules, CA) and blotted at 50 V for 2 hours. Proteins were transferred to a Trans-Blot Turbo Transfer Pack (BIO-RAD) using the Trans-Blot Turbo Transfer System V1.02 machine (BIO-RAD) at 2.5 A and 25 V. The membrane was incubated in 2.5% skim milk containing 0.5 % Tween 20 for an hour at room temperature. Primary antibodies against Calponin 3 (Santa Cruz Biotechnology, Inc., Santa Cruz, CA) (1:2000), Sorbin and SH3 Domain Containing 1 (Life Technologies, Carlsbad, CA) (1:1000), E-cadherin (Abcam, Cambridge, United Kingdom) (1:1000), and β-actin (Applied Biological Materials Inc., Richmond, BC, Canada) (1:5000) were introduced to the membrane and incubated at room temperature for 1 hour. Peroxidase-conjugated mouse or rabbit IgG antibody (Jackson Immunoresearch, West Grove, PA) (1:5000) was added as a secondary antibody and incubated at room temperature for 1 hour. Chemiluminescent working solution, WESTZOL (Intron Biotechnology), was decanted to the membrane. The membrane was exposed to Fuji RX film for 1-5 minutes.

Knockdown of CNN3 by Short Hairpin RNA Transduction

Forty thousand 293FT cells with 10 ml of DMEM supplied with 10% of FBS and 1% of penicillin streptomycin were seeded on a 100 pi tissue culture dish. After incubating for 24 hours at 37°C and 5% CO_2, the culture medium was changed to 10 ml of Opti-MEM, and short hairpin RNA targeting *CNN3* and control vector were treated using ViraSafe Lentiviral Packaging System, Pantropic (CELL BIOLABS, INC., San Diego, CA), and Lipofectamine 3000 (Invitrogen) in accordance with manufacturer's protocol. After 48 hours, the viral soup was harvested and filtered through a 0.45-μm pored filter (Sartorius Stedim Biotech SA, Göttingen, Germany). The harvested viral soup was aliquoted into a 1.5-ml tube and kept at −70°C. Fifty thousand peritoneal metastatic cells were seeded on 24-well tissue culture plate with 0.5 ml of RPMI1460 medium and incubated at 37°C in an atmosphere of 5% CO_2 and 95% air for 24 hours. Viral transduction was performed using ViraDuctin (CELL BIOLABS, INC., San Diego, CA) according to manufacturer's protocol.

Confocal Assay

Four thousand cells were seeded on chambered coverglass (Thermo Fisher Scientific, Waltham, MA). The chambered coverglass was designed to be hydrophilic, and no ECM component was treated before seeding. Once 70% confluency had been reached, cells were washed with cold DPBS three times. Then, cells were fixed and permeabilized with BD Cytofix/Cytoperm (BD Science, San Jose, CA). After cells were washed with washing solution (BD Science), DPBS containing 2% FBS (GE Healthcare Life Sciences, Buckinghamshire, UK) was applied for an hour. After cells were washed with cold DPBS, Calponin 3 (Santa Cruz Biotechnology, Santa Cruz, CA) (1:500) and E-cadherin antibody (Abcam, Cambridge, United Kingdom) (1:400) diluted in 0.05% of PBST was applied for 1.5 hours in room temperature. Thereafter, cells were washed with 0.05% of PBST, and Alexa 488 and Alexa 568 secondary antibodies (Thermo Fisher Scientific, Waltham, MA) (1:500) diluted in 0.05% of PBS.T were applied for an hour in room temperature. DAPI and Rhodamine-conjugated Phalloidin (Sigma-Aldrich, MO, USA) were diluted in distilled water and applied for 30 minutes in room temperature. Cells were washed with DPBS three times and applied under confocal microscope. LSM800 Confocal Laser Scanning Microscope and ZEN software (Carl Zeiss, Oberkochen, Germany) were used to analyze images. Digital resolution, scan speed, and the number of pictures averaged were set to 1024 × 1024, 40 seconds per one channel, and 8 pictures, respectively. Diverse magnifications were used in accordance with growth patterns and sizes of cells. Scale bar is inserted into each image processed. The intensity of each channel was fixed for comparing target protein expression between samples. The pictures were focused on the bottom of the fixed cells for investigating protruding region of cell colonies and the location of Calponin 3 and E-cadherin. *Z*-stacking was applied for SNU-2404 cell lines due to their aggregating nature. Distances from the initial focal point are indicated separately in Figure 3.

Gap Closure Migration Assay

Gap closure migration assay was performed using CytoSelect 24-Well Wound Healing Assay kit (CELL BIOLABS, INC., San Diego, CA) according to manufacturer's protocol. Briefly, SNU-2414B naïve, SNU-2414B shControl, and SNU-2414B shCNN3 cells were diluted to 2×10^5 cells/ml in RPMI1640 supplied with 10% of FBS and 1% of penicillin streptomycin. Once the inserts provided in the assay kit were put into each well of 24-well tissue culture plate, 500 μl of previously diluted cell solution was dispensed to each side of the insert, making a total of 1 ml of cell solution each well. After 24 hours of incubation at 37°C in an atmosphere of 5% CO_2 and 95% air, inserts were removed. Immediately, cells were washed with complete media twice. With 24-hour interval for 5 days, the wound closing process was recorded under phase contrast microscope. The closed wound area was calculated with ImageJ version 1.8.0. The whole

procedures were independently triplicated, and average closed wound area was analyzed using GraphPad Prism version 7.00 for Windows (GraphPad Software, La Jolla, CA).

3D Spheroid Cell Invasion Assay

3D spheroid cell invasion assay was performed using Cultrex 96-Well 3D Spheroid BME Cell Invasion Assay kit (Trevigen, Gaithersburg, MD) according to manufacturer's protocol. Dilute 1 × 10^6 cells per ml in cell culture medium. 10× Spheroid Formation ECM is thawed on ice at 4°C and diluted with RPMI1640 supplied with 10% of FBS and 1% of penicillin streptomycin chilled to 4°C. Spheroid Formation ECM solution is composed of proprietary mixture of extracellular matrix proteins derived from murine EHS sarcoma cells. Cells are resuspended in 1× Spheroid Formation ECM, and 50 μl of cell suspension is added to each well of the 3D Culture Qualified 96 Well Spheroid Formation Plate. Centrifuge at 200×*g* for 3 minutes at room temperature in a swinging bucket rotor, and incubate at 37°C in a tissue culture incubator for 72 hours to promote spheroid formation. After 72 hours, the 3D Culture Qualified 96 Well Spheroid Formation Plate is placed on ice for 15 minutes to cool wells. Working on ice, 50 μl of Invasion Matrix is added per well of the 3D Culture Qualified 96 Well Spheroid Formation Plate. The plate is centrifuged at 300×*g* at 4°C for 5 minutes in a swinging bucket rotor to eliminate bubbles and position spheroids within the Invasion Matrix towards the middle of the well. The plate is transferred to a tissue culture incubator set at 37°C for 1 hour to promote gel formation of the Invasion Matrix. After 1 hour, 100 μl of warm (37°C) cell culture medium is added containing 10% FBS as the chemoattractant. The spheroid in each well was photographed every 24 hours for 5 days under phase contrast microscope using the 4× objective. Images were analyzed using ImageJ version 1.8.0 (http://rsb.info.nih.gov/ij/). The area of the spheroid structure (μm^2) was analyzed using GraphPad Prism version 7.00 for Windows, (GraphPad Software, La Jolla, CA). The entire procedures were independently triplicated.

Statistical Analysis

Independent replicates refer to independent cell samples seeded, treated, and imaged on different days. Differences between effects of shCONT and shCNN3 were assessed with two-way ANOVA test. *P* values < .05 were considered statistically significant and indicated with asterisks using GraphPad Prism version 7.00 for Windows (GraphPad Software, La Jolla, CA). Microarray visualization and analysis were performed using R program version 3.3.1 (R Foundation for Statistical Computing, Vienna, Austria) with various packages including iplot, gplot, lattice, and RCircos. The microarray data were evaluated using Kruskal-Wallis test and Mann-Whitney *U* test with a Bonferroni correction for pathway analysis. The analysis for different mRNA species was performed using a two-tailed Spearman's rank correlation test, and differences were considered statistically significant at $^*P < .05$.

Results

General Characteristics of Cell Lines

The clinicopathologic characteristics of the cell lines are summarized in Table 1. The morphologies of each cell lines are described in figure legends (Figure 1*A*). All cell lines were free from bacteria or Mycoplasma contamination, and not cross-contaminated (Supplementary Table 23).

Whole Exome Sequencing Data Analysis

Thirty-one fundamental genes in developing CRC are selected from referring to previous research [13] (reference genes are listed in supplementary Table 23). SNU-2404 pair had the whole deletion of exon 3 in *CTNNB1* as confirmed by Western blotting and IGV program (Supplementary Figs. 1, 2). None of the TP53 mutations was located in hot spots containing CpG dinucleotides, and all mutations were homozygous. Detailed results of the whole exome sequencing are summarized in Supplementary Tables 1-5. Moreover, shared mutations in peritoneal metastasis cell lines were screened (Supplementary Tables 6-8). Only one missense mutation of CYP2A7 (c.181T>A/p.Phe61Ile) was exclusively shared in all three peritoneal metastatic cancer cell lines.

Microarray Data Analysis

Two-folds change classification was used to select distinctly expressed genes in peritoneal metastasis cell lines. The number of up- and downregulated genes with their intersection between two different peritoneal metastasis cell lines is summarized in Figure 1, *B* and *C*. The number of upregulated genes in the intersection between SNU-2404 set and other two pairs was much lower than that of shared genes between SNU-2335 set and SNU-2414 set (Figure 1*B*). It was reencapsulated in the circos-plot presenting distinct mRNA expressions of classified genes (Figure 1*H*). There were multiple genomic regions such as 4q24-4q26, 5p15.33-5p14.1, 6p22.3-6p22.1, and 7p21.3 in which genes identified from SNU-2404 pair were reversely regulated in SNU-2335 and SNU-2414 sets. Given that the adherent growth pattern of SNU-2404A is changed to floating aggregates in SNU-2404B, it could be assumed that SNU-2404A had different kinds of alternation in extracellular matrix binding molecules or/and epithelial mesenchymal transition factors. This prospect leads to pathway analysis to investigate which signaling pathways are aberrated in peritoneal metastasis (Figure 1, *I*, *J*, *K* and Supplementary Figs. 5-11). The result from the pathway analysis certified the assumption that the SNU-2404 set has distinct deregulated pathways from the other two pairs. Both SNU-2335 and SNU-2414 sets had activated focal adhesion, MAPK, and TGF-beta signaling (Figure 1, *I* and *K*). On the contrary, SNU-2404 set had inhibited ECM receptor binding, bile secretion, and small cell signaling (Figure 1*J*). There were five upregulated and two downregulated genes in all three peritoneal metastasis cell lines (Table 2, Figure 1, *B* and *C*), and these genes may play a role in connecting diverse deregulated pathways. For those seven genes, a heatmap was drawn to visualize fold changes (Figure 1*G*). Their expressions in mRNA level were reconfirmed by RT-PCR (Figure 1*E*). *CNN3* became gene of interest since its mRNA level was remarkably augmented in SNU-2404B cells (10.6-folds) compared to that of SNU-2335D (2.5-folds) and SNU-2414B cells (4.2-folds) and was likely to explain the morphologic change of the SNU-2404 pair. To further classify primary cell lines and metastatic cell lines for target gene selection, 156 probe sets with $^*P<.05$ using paired *t* test were selected. Among them, 15 genes with the highest scores in primary and metastatic classes were identified (Figure 1*D*). *CNN3, SORBS1,* and *TRY6* were identified in both fold change selection and classification using a probe set, and their protein levels in isolated peritoneal pairs were confirmed with Western blotting. Protein expression of *TRY6* was not detectable, and the only results from *CNN3* and *SORBS1* were shown (Figure 1*F*). Interestingly, *SORBS1* band was absent in SNU-2335D, while it was highly increased in SNU-2335E, which is an ovarian metastasis cancer cell line. On the

other hand, *CNN3* band was clearly amplified in SNU-2335D compared to SNU-2335A, and SNU-2335E had similar expression level with SNU-2335A. Therefore, *CNN3* was pursued for specific marker for peritoneal metastasis, and functional study was continued.

CNN3 Expression Analysis in Colorectal Cancer Cell Lines by RT-PCR and Western Blotting

The expression of *CNN3* in mRNA level was examined in 32 CRC cell lines (Figure 2*A*). Of the used 32 CRC cell lines, molecular profiles of 14 CRC cell lines were deposited in the canSAR database (https://cansar.icr.ac.uk). Mutational features of 14 cell lines were analyzed in accordance with their mRNA levels and described in the discussion section. The mRNA level of *CNN3* was distinctly higher in SNU-769A (lymph node metastasis) than SNU-769B (primary CRC tissue). In order to verify if the Calponin 3 is amplified in other metastasis pair of CRC cell lines, SW-480, SW-620, KM12C, KM12SM, and KM12L4 cell lines were obtained from Korean Cell Line Bank. Consistently, Calponin 3 was increased in metastatic cancer cell lines (Figure 2*B*).

3D Spheroid Cell Invasion Assay and Gap Closure Migration Assay

In order to further investigate the role of Calponin 3 in peritoneal metastasis cancer cells, short hairpin RNA targeting *CNN3* (shCNN3) was transducted to the peritoneal metastasis cell lines. SNU-2335 pair was excluded since knockdown of Calponin 3 caused cell death. 3D spheroid cell invasion assay signified that knockdown

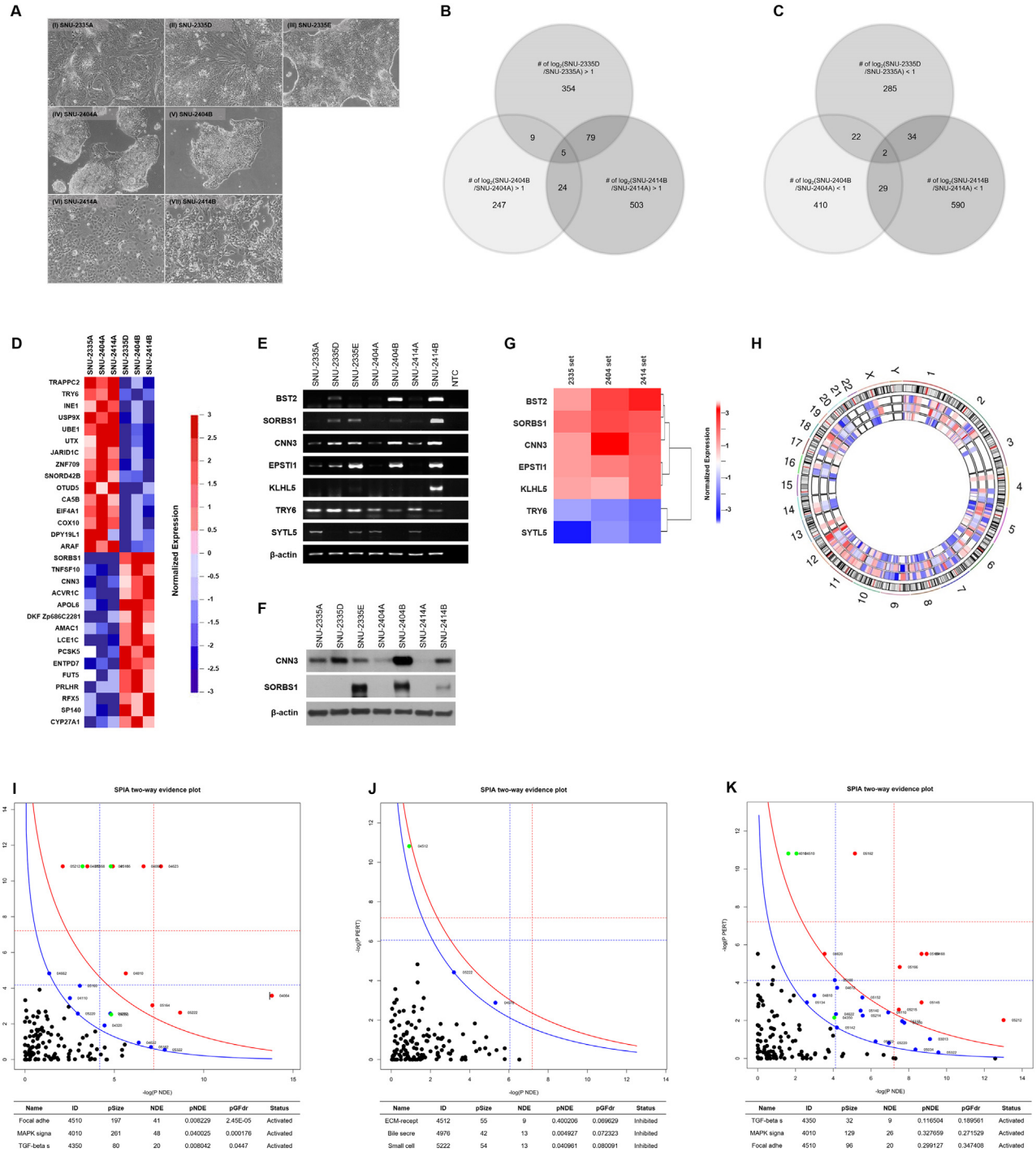

Table 2. Genes Selected from Microarray Data Analysis

Probe Set ID	Symbol	Gene Description	GO Term Function	Fold Change		
				SNU-2335D	SNU-2404B	SNU-2414B
Upregulated genes in all three cell lines						
7917885	CNN3	calponin 3, acidic	actin binding	2.5	10.6	4.2
7935188	SORBS1	sorbin and SH3 domain containing 1	actin binding	3.5	5.3	4.6
7971296	EPSTI1	epithelial stromal interaction (breast)		2.5	3.1	3.9
8035304	BST2	bone marrow stromal cell antigen 2	signal transducer activity	2.5	5.5	8.2
8094625	KLHL5	kelch-like 5 (Drosophila)	actin binding	2.3	2.1	4
Probe Set ID	Symbol	Gene Description	Function	Fold Change		
				SNU-2335D	SNU-2404B	SNU-2414B
Downregulated genes in all three cell lines						
8136790	TRY6	trypsinogen C		-2.2	-2.6	-4
8166747	SYTL5	synaptotagmin-like 5	protein binding	-8.5	-2.7	-3.6

Log2-fold change was computed based on the mRNA expressions of metastatic CRC cell lines (SNU-2335D, SNU-2404B, and SNU-2414B) compared to primary CRC cell lines (SNU-2335A, SNU-2404A, and SNU-2414A).

of Calponin 3 resulted in decreased invasiveness in both SNU-2404 (Figure 2*D*) and SNU-2414 pairs (Figure 2*E*). Cell proliferation was measured in parallel with 3D spheroid cell invasion assay to distinguish invasion ability from the growth rate in both SNU-2404 (Figure 2*F*) and SNU-2414 set (Figure 2*G*). Besides, peritoneal metastasis cells with downregulated Calponin 3 aggregated more tightly, and the spheroid maintained intact round shape compared to parental peritoneal metastasis cells (Figure 2, *H* and *I*). SNU-2404 set was ruled out for gap closure migration assay for their floating aggregate nature. In parallel with 3D spheroid cell invasion assay, downregulating Calponin 3 in SNU-2414B hindered the wound closing rate compared to SNU-2414B naive and SNU-2414B with control vector (Figure 2, *J* and *L*). Entire procedure was independently triplicated and averaged. Cell proliferation was measured in parallel with wound healing assay to distinguish migration ability from growth rate (Figure 2*K*).

Calponin 3 Analysis in Established CRC Cell Lines by Immunofluorescence

The location and relative expression of Calponin 3 were examined by immunofluorescence. Consistent with prior findings, cell lines derived from peritoneal metastasis CRC had augmented Calponin 3 compared to the primary CRC cell lines (Figure 3*A*). In SNU-2335 and SNU-2414 sets, colocalization of Calponin 3 and F-actin was mostly restricted to intercellular junction, and Calponin 3 was most prominent at the edge of the colonized cell population (Figure 3, *A*, *B* and *C*).

Referring to 3D invasion assay, knockdown of Calponin 3 resulted in tightly packed spheroid in both SNU-2404B and SNU-2414B, which led to the potential relationship of Calponin 3 and E-cadherin. Remarkably, knockdown of Calponin 3 in SNU-2414B cell line increased E-cadherin level in both Western blotting (Figure 2*C*) and immunofluorescence assay (Figure 4*A*). This was observed in SNU-2404B cell line in Western blotting as well (Figure 2*C*). To obtain entirety of floating SNU-2404B cell colonies, *Z*-stacking was applied. Within a single spheroid population, Calponin 3 was expressed in outer region of the SNU-2404B shCONT aggregate compared to E-cadherin (Figure 4, *B* and *C*). SPIA pathway analysis indicated SNU-2404 set had inhibited ECM binding signaling (Figure 1*J*), and this result may imply that Calponin 3 plays a role in impeding ECM binding of SNU-2404B cells. Downregulating Calponin 3 barely affected F-actin structure in both SNU-2404 and SNU-2414 sets (Supplementary Figure 4, *A* and *B*). Nevertheless, it could be

Figure 1. Selection and verification of distinct gene expressions and aberrated signaling pathways in peritoneal seeding cell lines. (A) Phase-contrast microscopy of paired colorectal cancer cell lines before being applied to whole exome sequencing and microarray. The majority of tumor cells displayed a polygonal shape and had round-to-oval nuclei with prominent single-to-double nucleoli. (AI) SNU-2335A, (AII) SNU-2335D, and (AIII) SNU-2335E grew as monolayers composed of epithelial cell islands. (AIV) SNU-2404A grew as tightly packed floating cell aggregates. (AV) SNU-2404B, which was derived from ascending colon mass, grew as irregular floating clumps. (AVI) SNU-2414A and (AVII) SNU-2414B proliferated as islands of tightly packed epithelial cells and eventually formed dense monolayers. (B) Venn diagram shows the overlap of upregulated genes and (C) downregulated genes using two-fold change threshold. (D) Heatmap indicating classified primary and metastatic cell lines was drawn with 156 probe sets having $*P < .05$ by using paired *t* test. Among them, 15 genes with the highest score in primary and metastatic classes were identified. (E) The mRNA expressions of classified seven genes in established primary CRC and peritoneal cancer cell lines. (F) The protein levels of *CNN3* and *SORBS1* in the primary CRC and peritoneal cancer cell lines. (G) Heatmap represents the selected seven genes that were differently expressed in all three metastatic CRC cell lines. Expression level was converted to log2 scale. Each selected gene was clustered in accordance with similarity of expression levels. (H) Circos plot shows chromosomal area where certain sets of genes were up- or downregulated in all three metastatic cell lines. The outermost circle represents the entire human chromosome (hg19). The second, third, and fourth outermost circles represent chromosomal regions of SNU-2335, SNU-2404, and SNU-2414 sets, respectively. (I) SPIA evidence plot for the microarray result of SNU-2335 set. Each pathway is represented by one dot. The pathways at the right of the red curve are significant after Bonferroni correction. The pathways at the right of the blue curve line are significant after a FDR correction of the global *P* values. (J) SPIA evidence plot for the microarray result of SNU-2404 set. Each pathway is represented by one dot. The pathways at the right of the red curve are significant after Bonferroni correction. The pathways at the right of the blue curve line are significant after a FDR correction of the global *P* values. (K) SPIA evidence plot for the microarray result of SNU-2414 set. Each pathway is represented by one dot. The pathways at the right of the red curve are significant after Bonferroni correction. The pathways at the right of the blue curve line are significant after a FDR correction of the global *P* values.

observed that SNU-2414B shCNN3 cells had more circular shape than SNU-2414B shCONT cells (Supplementary Figure 4*A*).

Discussion

Recently, there have been many reports regarding the use of novel gene markers for diagnostic tools, chemotherapeutic targets, and predicting prognosis [14–18]. Although genetic studies of colorectal carcinogenesis have focused on the differences between normal colonic mucosa and primary carcinomas [14], there are few studies on the genetic alteration of primary carcinomas to peritoneal metastases. Diep et al. [9] profiled that peritoneal carcinomatoses and liver metastases usually have more DNA copy number changes than

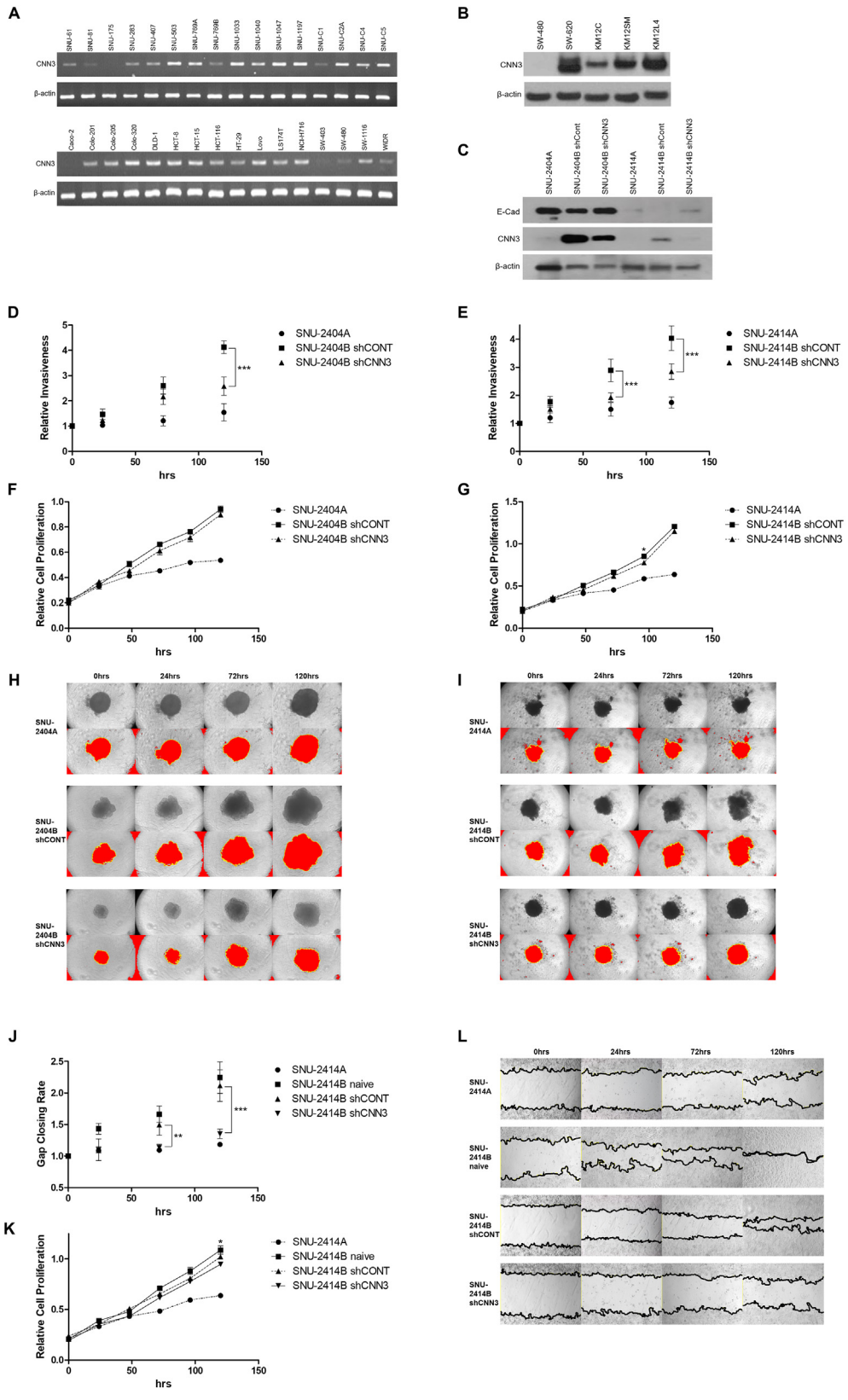

original lesions. Kleivi et al. reported that chromosome arm 5p gains are common in peritoneal carcinomatoses, and 20 genes (including PTGER4, SKP2, and ZNF622) mapping in this region were overexpressed in the tumors [10]. The purpose of this study was to find novel markers for identifying peritoneal metastases in CRC. We identified 117 upregulated genes (Supplementary Table 19) and 87 downregulated genes (Supplementary Table 20) in more than two metastatic cell lines by microarray. Five upregulated (*CNN3*, *SORBS1*, *BST2*, *EPSTI1*, and *KLHL5*) and two downregulated genes (*TRY6* and *STYL5*) were differentially expressed in all three metastatic cell lines (Table 2).

Microarray Data Analysis

According to Gene Ontology term analysis, three upregulated genes (*CNN3*, *SORBS1* and *KLHL5*) in the three peritoneal metastasis cell lines were associated with actin binding (Table 2). *KLHL5* was only present in SNU-2414B, whereas *CNN3* and *SORBS1* were detected in all peritoneal metastasis cell lines (Figure 1*E*). *KLHL5* gene was reported to be related with various cellular processes, such as actin cytoskeleton interaction, cytoplasmic sequestration of transcription factors, and cell morphology [19]. Given that the growth pattern of SNU-2414B (monolayer) was different from that of SNU-2335D (multilayer) and SNU-2404B (floating), *KLHL5* might be related to the contact inhibition. The exclusive expression pattern of *BST2* and *STYL5* in SNU-2335 triple was noteworthy. *BST2* was present only in SNU-2335D, while *STYL5* was expressed in SNU-2335A and SNU-2335E (Figure 1*E*). It was reported that the expression of *STYL5* in mRNA level was increased in invasive breast carcinoma in response to estradiol, and it affected diverse aspects of vesicle trafficking including exocytosis [20]. Given that SNU-2335E was derived from a Krukenberg tumor mass, estradiol may be responsible for the *SYTL5* expression in SNU-2335E. Furthermore, *SYTL5* is known as an effector molecule that specifically binds and regulates the GTP-bound form of the GTPase RAB27A/B [21]. Recently, Dong W et al. reported that decreased expression of RAB27A/B correlates with metastasis in colorectal cancer [22]. *SYTL5* was exclusively absent in all peritoneal metastasis cell lines in mRNA level (Figure 1*E*). Our findings may indicate that *SYTL5* deregulates RAB27A/B in primary CRC and promotes proceeding to peritoneal metastasis. *BST2* has been reported to mediate metastasis in several types of cancer [23,24] Walter-Yohrling et al. revealed that *BST2* expression was highly augmented in metastatic ovarian cancer [25]. Nevertheless, in SNU-2335 set, *BST2* expression was selectively increased in peritoneal metastasis, and SNU-2335E was analogous to SNU-2335A in both microarray and RT-PCR. The absence of *BST2* in Krukenberg tumor mass is to be elucidated.

Whole Exome Sequencing Data Analysis

Mutations that were previously reported in developing metastatic colorectal cancer were screened. The proposed functions of mutations and references are listed in Supplementary Table 9 [26–32]. CTNNB1 codes β-catenin, which plays a major role in Wnt signaling, and its status is closely related to distant metastasis. SNU-2335A harbored c.1974C>A/p.Asp658Glu missense mutation in CTNNB1, which was not detected in its paired metastatic cell lines. The c.1974C>A/p.Asp658Glu missense mutation was reported previously, but its functional role has not been discovered. Although all cell lines had MSH3 missense mutations, cells were identified as microsatellite stable. According to dbSNP database, clinical significance of one mutation (c.235A>G/p.Ile79Val) was known to be benign, and that of other two mutations (c.2846A>G/p.Gln949Arg and c.3133G>A/p.Ala1045Thr) was unknown. Even though c.3133G>A/p.Ala1045Thr mutation was reported to increase cancer risk in multiple organs such as colorectal cancer, breast cancer, prostate cancer, ovarian cancer, and esophageal cancer [33], none was reported to be related with inactivation of MSH3. One missense mutation in the CYP2A7 was shared in all three peritoneal metastatic cell lines. CYP2A7 is expressed mainly in liver tissue, and its role in colorectal cancer remains unclear. We took advantage of publically available cancer cell line database (canSAR) and drew comparison between mutational status of CYP2A7 gene and CNN3 expression level. Although the genomic positions of mutation were various, missense mutations of CYP2A7 were found in SNU-1040 (c.306C>T/p.Gly102Gly), SNU-C5 (c.164A>T/p.Tyr55Phe), and HCT-15 (c.230G>A/p.Arg77Gln) cell lines among 14 available CRC cell lines from the canSAR database. These cell lines had relatively high CNN3 level compared to the rest of 11 cell lines analyzed (Figure 2*A*). This may imply that mutational status of CYP2A7 gene is connected to augmented CNN3 expression.

We also compared our WES data to findings by Nicholas E. Navin's lab which reported genomic alterations in distant metastases

Figure 2. The potential involvement of Calponin 3 in cell invasion and migration. (A) The mRNA level of *CNN3* in 32 previously reported colorectal cancer cell lines. Amplified CNN3 fragments were absent in 3 of the 32 CRC cell lines (i.e., in SNU-175, Caco-2, and SW-403). Of the remaining 29 cell lines, 10 (SNU-61, SNU-81, SNU-283, SNU-407, SNU-769B, SNU-C1, Colo-201, HT-29, SW-480, and WiDr) had relatively low expressions, whereas 19 of the CRC cell lines (SNU-503, SNU-769A, SNU-1033, SNU-1040, SNU-1047, SNU-1197, SNU-C2A, SNU-C4, SNU-C5, Colo-205, Colo-320, DLD1, HCT-8, HCT-15, HCT-116, LoVo, LS174T, NCI-H716, and SW-1116) exhibited strong expressions. (B) The protein level of CNN3 in two pairs of metastasis colorectal cancer cell lines. Calponin 3 was increased in metastatic CRC cell lines (SW-620, KM12SM, and KM12L4) than primary CRC cell lines (SW-480 and KM12C). (C) The efficacy of short hairpin RNA to knockdown Calponin 3 was accessed with Western blotting. The E-cadherin level was confirmed in comparison to Calponin 3. E-cadherin and Calponin 3 were inversely related. The result of 3D spheroid cell invasion assay indicated that knockdown of Calponin 3 resulted in decreased invasiveness in both (D) SNU-2404 and (E) SNU-2414 set. Cell proliferation was measured in parallel with 3D spheroid cell invasion assay to distinguish invasion ability from the growth rate in both (F) SNU-2404 and (G) SNU-2414 set. Error bars and *P* values are calculated with independently repeated experiments ($N = 3$, $^{*}P<.05$, $^{***}P<.001$) Besides, peritoneal metastasis cells with downregulated Calponin 3 formed spheroid in different shape from original peritoneal metastasis cells. Cells were aggregated more tightly, and the spheroid maintained intact round shape compared to original peritoneal metastasis cells in both (H) SNU-2404 and (I) SNU-2414 set. (J, L) Downregulating Calponin 3 in SNU-2414B hindered the wound closing rate compared to SNU-2414B naive and SNU-2414B with control vector. The experiment was triplicated and averaged. (K) Cell proliferation was measured in parallel with wound healing assay to distinguish migration ability from growth rate. The experiment was triplicated and averaged. Error bars and *P* values are calculated with independently repeated experiments ($N = 3$, $^{*}P<.05$, $^{**}P<.01$, $^{***}P<.001$)

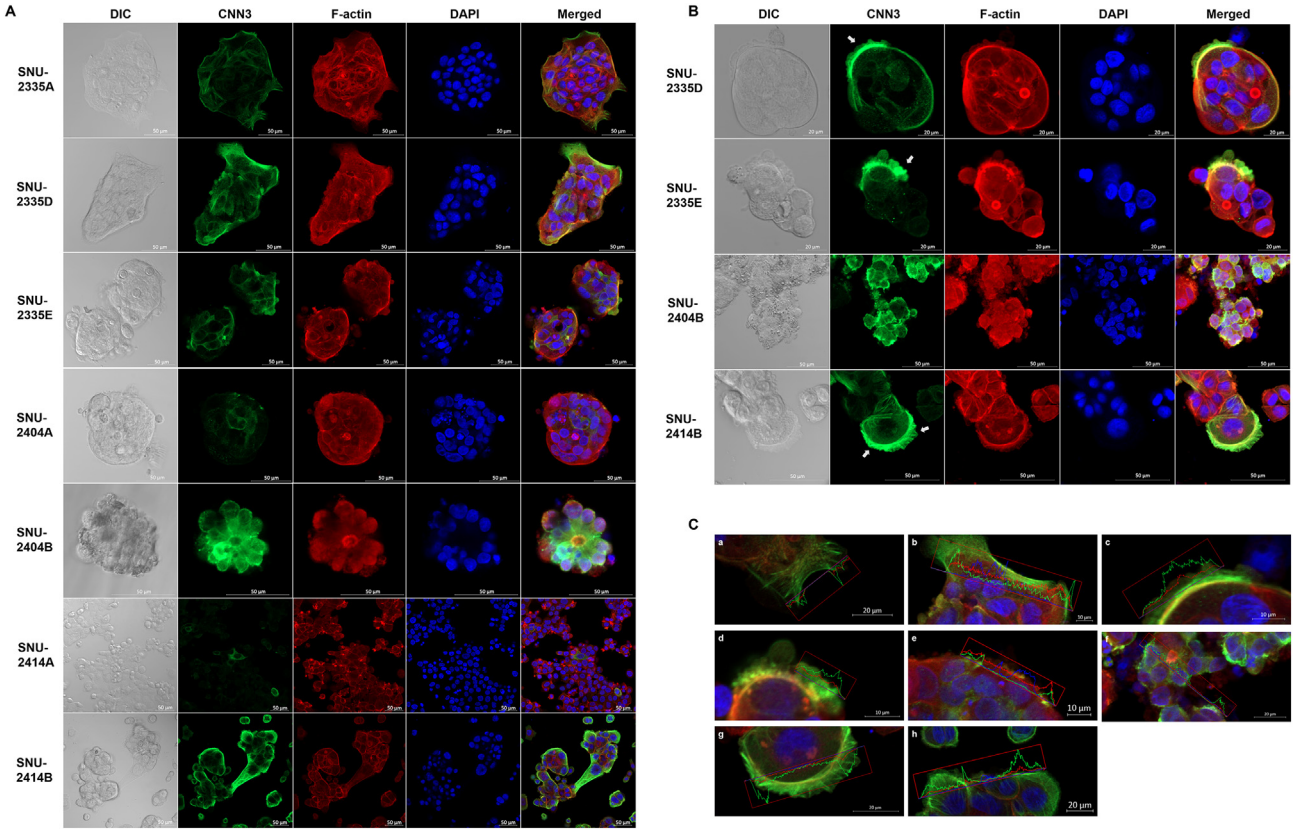

Figure 3. The expression of Calponin 3 is enhanced at the edge of the colonized cell population. (A) Confocal images represent relative expression and localization of Calponin 3 (green) *in vitro*. Red and blue indicate F-actin and nucleus, respectively. Calponin 3 was distinct at the edge of the colonized cell population. Scale bar is inserted into each image. (B) Confocal microscopy of metastatic peritoneal seeding cell lines. Metastatic cancer cell lines showed recruitment of Calponin 3 at the protruding regions of the colonized cell population (indicated by arrow). (C) Enlarged images from A and B indicated that the intensity of Calponin 3 (green) signal is prominent compared to F-actin (red) signal. (a) SNU-2335A. (b) (c) SNU-2335D. (d) SNU-2335E. (e) SNU-2404A. (f) SNU-2404B. (g, h) SNU-2414B. (SNU-2414A was omitted since the intensity of Calponin 3 was too low).

in a single cell level [34]. They detected 13 mutations that were exclusively found in primary CRC and 37 mutations that were selectively harbored in metastatic cells by deep-exome sequencing. Although genomic positions of each mutation varied, 5 genes were found to have missense mutations in our primary CRC cell lines, and 9 genes were found to have missense mutations in our peritoneal metastasis cell lines (Supplementary Table 10-15). They also reported genes that mediated clonal evolution in the metastatic site by ultra-deep targeted sequencing. We screened the variant allele frequency of those genes in our primary CRC and peritoneal metastasis cell lines (Supplementary Tables 16-18). In SNU-2414 set, PIK3CG and LINGO2 mutations were detected in primary CRC, and SPEN mutation was found in metastasis cell line, which was concordant with their findings. Moreover, variant allele frequencies of three missense mutations in EYS gene (c.5705A>T, c.4256T>C, c.1712A>G) were changed from ~0.5 in SNU-2414A to 1 in SNU-2414B, which may indicate clonal evolution at metastatic site. The potential role of EYS gene in metastasis should be elucidated.

CNN3 as a Potential Metastasis Marker

As one of three isoforms (basic/h1-calponin, neutral/h2-calponin, and acidic/h3-calponin) in the calponin family that functions as calmodulin and F-actin binding partners, Calponin 3 is expressed in smooth muscle and nonmuscle cells [35]. While the role of the calponin family in regulating smooth muscle contractility has been extensively investigated, the function and regulation in nonmuscle cells are much less understood. Recent studies have demonstrated that calponin family plays a regulatory role in nonmuscle cell motility, which makes calponin family as an attractive target for controlling cell proliferation, metastases, and cancer treatment [36].

In order to confirm the expression profile in the original histological patient samples, we obtained very initial passages of each cell line (passage 1 or 2) and checked the differential expression of candidates in mRNA level (Supplementary Figure 3*B*). Expression profiles of all seven identified candidates in the initial passages of each cell line were analogous to passaged samples. Calponin 3 was the main target of our research and was confirmed in protein level as well (Supplementary Figure 3*C*). In all three pairs, Calponin 3 was augmented in the peritoneal metastasis cell lines.

3D spheroid cell invasion assay and Western blotting indicated that the E-cadherin level is inversely related to Calponin 3 expression (Figure 2*C*). The peritoneal metastatic cascade begins with the detachment of singular or clumps of tumor cells from the primary tumor [37]. Spontaneous exfoliation of malignant cells can be promoted by the downregulation of intracellular adhesion molecules on the tumor cell surfaces, more specifically E-cadherin [4]. Calponin

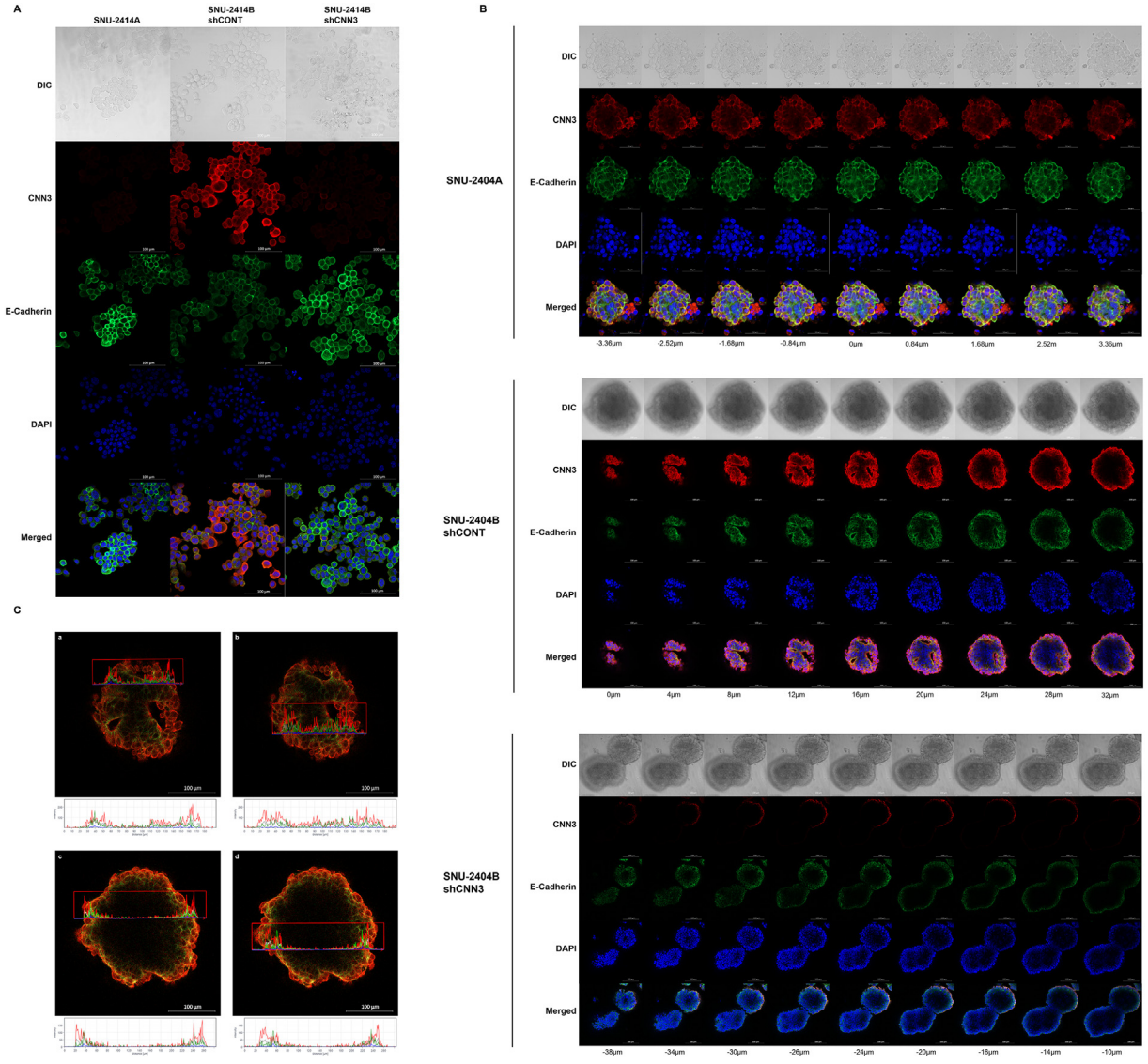

Figure 4. Immunofluorescence was performed to examine the relationship between Calponin 3 and E-cadherin. (A) Knockdown of Calponin 3 in SNU-2414B cell line increased E-cadherin expression. (B) To obtain entirety of floating SNU-2404B cell colonies, *Z*-stacking was applied. Within a single spheroid population, Calponin 3 was mostly located in the outer shell of the spheroid, and E-cadherin remained in the inner shell of the aggregate. (C) The intensity of Calponin 3 (Red) and E-Cadherin (Green) signals was measured and graphed through one axis. (a, b) Two random points were selected on the mid-transverse section of SNU-2404B shCONT spheroid image (16 μm). Peaks on the graph indicated that Calponin 3 signal is located in the outer region compared to E-cadherin signal. (c, d) Two random points were selected on the bottom-transverse section of SNU-2404B shCONT spheroid image (32 μm). Peaks on the graph indicated that Calponin 3 signal is located outer region compared to E-cadherin signal.

3 may participate in the initial dissemination of tumor cell from the primary tumor by downregulating the level of E-cadherin. Moreover, confocal images of SNU-2404 and SNU-2414 sets indicated that Calponin 3 was mostly located in outer boundaries, whereas E-cadherin remained at the cellular surface of inner cells within a colonized cell population (Figure 4, *A* and *C*). It was previously reported that the Calponin 3 was upregulated in response to mechanical stress such as high fluid pressure around tumor mass [38,39]. Cells at the outmost region of the cell colonies experience sheer force, which may account for the selective expression of Calponin 3. In terms of the role of Calponin 3 in peritoneal metastasis cascade, the level of Calponin 3 within cells at the outer shell of tumor clumps can be increased by mechanical stress around the tumor mass, and augmented Calponin 3 deregulates the expression of E-cadherin to promote spontaneous tumor cell shedding from the primary tumor. The mechanism of Calponin 3 to decrease E-cadherin level should be further investigated. Moreover, the formation of actin-rich membrane protrusions such as lammelipodia and filipodia is important to peritoneal transport of detached tumor cells [40]. The confocal images of SNU-2414 set indicated that the protruding region at the edge of SNU-2414B shCNN3 was significantly diminished compared to SNU-2414B shCONT (Supplementary Figure 4*A*). This may imply that CNN3 took part in lamellipodia formation.

Taken together, we propose that the higher Calponin 3 expression may play a role in increasing CRC cell invasion partially due to its association with lower E-cadherin level, and suggest that Calponin 3 can be linked to a positive function in the peritoneal metastasis of CRC.

Supplementary data to this article can be found online at https://doi.org/10.1016/j.tranon.2018.07.014.

Ethics Approval and Consent to Participate

The study protocol was approved by the Institutional Review Board of Seoul National University Hospital (IRB No. H-1102-098-357). The study was performed in accordance with the Declaration of Helsinki.

Consent for Publication

Not applicable.

Availability of Data and Materials

Data supporting the results reported in the article can be accessed by the authors upon demand.

Conflict of Interest

The authors declare no conflict of interest.

Authorship

S. C. designed and performed the experiment and write the manuscript. C. W. performed surgical removal of primary and peritoneal metastasis tumor and helped designed the experiment. S. G. helped analyze microarray data. Y. A. helped knock down of Calponin 3. B. C. helped design the invasion assay. Y. K. provided CRC cell lines. S. Y. helped design the experiment. J. L. designed the experiment. J. G. designed the experiment.

Acknowledgements

Not applicable.

References

[1] Jung KW, Won YJ, Oh CM, Kong HJ, Lee DH, and Lee KH (2017). Cancer statistics in Korea: incidence, mortality, survival, and prevalence in 2014. *Cancer Res Treat* **49**, 292–305.

[2] Shih W, Chetty R, and Tsao MS (2005). Expression profiling by microarrays in colorectal cancer (Review). *Oncol Rep* **13**, 517–524.

[3] Brabletz T, Hlubek F, Spaderna S, Schmalhofer O, Hiendlmeyer E, Jung A, and Kirchner T (2005). Invasion and metastasis in colorectal cancer: epithelial-mesenchymal transition, mesenchymal-epithelial transition, stem cells and beta-catenin. *Cells Tissues Organs* **179**, 56–65.

[4] Hirohashi S (1998). Inactivation of the E-cadherin-mediated cell adhesion system in human cancers. *Am J Pathol* **153**, 333–339.

[5] Heath RM, Jayne DG, O'Leary R, Morrison EE, and Guillou PJ (2004). Tumour-induced apoptosis in human mesothelial cells: a mechanism of peritoneal invasion by Fas Ligand/Fas interaction. *Br J Cancer* **90**, 1437–1442.

[6] Bracke ME (2007). Role of adhesion molecules in locoregional cancer spread. *Cancer Treat Res* **134**, 35–49.

[7] Muller J and Yoshida T (1995). Interaction of murine peritoneal leukocytes and mesothelial cells: in vitro model system to survey cellular events on serosal membranes during inflammation. *Clin Immunol Immunopathol* **75**, 231–238.

[8] Kataoka H, Tanaka H, Nagaike K, Uchiyama S, and Itoh H (2003). Role of cancer cell-stroma interaction in invasive growth of cancer cells. *Hum Cell* **16**, 1–14.

[9] Diep CB, Teixeira MR, Thorstensen L, Wiig JN, Eknaes M, Nesland JM, Giercksky KE, Johansson B, and Lothe RA (2004). Genome characteristics of primary carcinomas, local recurrences, carcinomatoses, and liver metastases from colorectal cancer patients. *Mol Cancer* **3**, 6.

[10] Kleivi K, Lind GE, Diep CB, Meling GI, Brandal LT, Nesland JM, Myklebost O, Rognum TO, Giercksky KE, and Skotheim RI, et al (2007). Gene expression profiles of primary colorectal carcinomas, liver metastases, and carcinomatoses. *Mol Cancer* **6**, 2.

[11] Lemoine L, Sugarbaker P, and Van der Speeten K (2016). Pathophysiology of colorectal peritoneal carcinomatosis: role of the peritoneum. *World J Gastroenterol* **22**, 7692–7707.

[12] Ku JL, Shin YK, Kim DW, Kim KH, Choi JS, Hong SH, Jeon YK, Kim SH, Kim HS, and Park JH, et al (2010). Establishment and characterization of 13 human colorectal carcinoma cell lines: mutations of genes and expressions of drug-sensitivity genes and cancer stem cell markers. *Carcinogenesis* **31**, 1003–1009.

[13] *Comprehensive molecular characterization of human colon and rectal cancerNature* **487**, 330–337.

[14] Buckhaults P, Rago C, St Croix B, Romans KE, Saha S, Zhang L, Vogelstein B, and Kinzler KW (2001). Secreted and cell surface genes expressed in benign and malignant colorectal tumors. *Cancer Res* **61**, 6996–7001.

[15] Kitahara O, Furukawa Y, Tanaka T, Kihara C, Ono K, Yanagawa R, Nita ME, Takagi T, Nakamura Y, and Tsunoda T (2001). Alterations of gene expression during colorectal carcinogenesis revealed by cDNA microarrays after laser-capture microdissection of tumor tissues and normal epithelia. *Cancer Res* **61**, 3544–3549.

[16] Koehler A, Bataille F, Schmid C, Ruemmele P, Waldeck A, Blaszyk H, Hartmann A, Hofstaedter F, and Dietmaier W (2004). Gene expression profiling of colorectal cancer and metastases divides tumours according to their clinicopathological stage. *J Pathol* **204**, 65–74.

[17] Williams NS, Gaynor RB, Scoggin S, Verma U, Gokaslan T, Simmang C, Fleming J, Tavana D, Frenkel E, and Becerra C (2003). Identification and validation of genes involved in the pathogenesis of colorectal cancer using cDNA microarrays and RNA interference. *Clin Cancer Res* **9**, 931–946.

[18] Ichikawa Y, Ishikawa T, Takahashi S, Hamaguchi Y, Morita T, Nishizuka I, Yamaguchi S, Endo I, Ike H, and Togo S, et al (2002). Identification of genes regulating colorectal carcinogenesis by using the algorithm for diagnosing malignant state method. *Biochem Biophys Res Commun* **296**, 497–506.

[19] Xu J, Gu S, Wang S, Dai J, Ji C, Jin Y, Qian J, Wang L, Ye X, and Xie Y, et al (2003). Characterization of a novel splicing variant of KLHL5, a member of the kelch protein family. *Mol Biol Rep* **30**, 239–242.

[20] Wright PK, May FE, Darby S, Saif R, Lennard TW, and Westley BR (2009). Estrogen regulates vesicle trafficking gene expression in EFF-3, EFM-19 and MCF-7 breast cancer cells. *Int J Clin Exp Pathol* **2**, 463–475.

[21] Kuroda TS, Fukuda M, Ariga H, and Mikoshiba K (2002). Synaptotagmin-like protein 5: a novel Rab27A effector with C-terminal tandem C2 domains. *Biochem Biophys Res Commun* **293**, 899–906.

[22] Dong W, Cui J, Yang J, Li W, Wang S, Wang X, Li X, Lu Y, and Xiao W (2015). Decreased expression of Rab27A and Rab27B correlates with metastasis and poor prognosis in colorectal cancer. *Discov Med* **20**, 357–367.

[23] Hundemer M, Schmidt S, Condomines M, Lupu A, Hose D, Moos M, Cremer F, Kleist C, Terness P, and Belle S, et al (2006). Identification of a new HLA-A2-restricted T-cell epitope within HM1.24 as immunotherapy target for multiple myeloma. *Exp Hematol* **34**, 486–496.

[24] Cai D, Cao J, Li Z, Zheng X, Yao Y, Li W, and Yuan Z (2009). Up-regulation of bone marrow stromal protein 2 (BST2) in breast cancer with bone metastasis. *BMC Cancer* **9**, 102.

[25] Walter-Yohrling J, Cao X, Callahan M, Weber W, Morgenbesser S, Madden SL, Wang C, and Teicher BA (2003). Identification of genes expressed in malignant cells that promote invasion. *Cancer Res* **63**, 8939–8947.

[26] Jang EK, Song DE, Sim SY, Kwon H, Choi YM, Jeon MJ, Han JM, Kim WG, Kim TY, and Shong YK, et al (2014). NRAS codon 61 mutation is associated with distant metastasis in patients with follicular thyroid carcinoma. *Thyroid* **24**, 1275–1281.

[27] Ghidini M, Personeni N, Bozzarelli S, Baretti M, Basso G, Bianchi P, Tronconi MC, Pressiani T, Grizzi F, and Giordano L, et al (2016). KRAS mutation in lung metastases from colorectal cancer: prognostic implications. *Cancer Med* **5**, 256–264.

[28] Ormanns S, Neumann J, Horst D, Kirchner T, and Jung A (2014). WNT signaling and distant metastasis in colon cancer through transcriptional activity of nuclear beta-Catenin depend on active PI3K signaling. *Oncotarget* **5**, 2999–3011.

[29] Morin PJ, Sparks AB, Korinek V, Barker N, Clevers H, Vogelstein B, and Kinzler KW (1997). Activation of beta-catenin-Tcf signaling in colon cancer by mutations in beta-catenin or APC. *Science* **275**, 1787–1790.

[30] Grimm WA, Messer JS, Murphy SF, Nero T, Lodolce JP, Weber CR, Logsdon MF, Bartulis S, Sylvester BE, and Springer A, et al (2016). The Thr300Ala variant in ATG16L1 is associated with improved survival in human colorectal cancer and enhanced production of type I interferon. *Gut* **65**, 456–464.

[31] Le Rolle AF, Klempner SJ, Garrett CR, Seery T, Sanford EM, Balasubramanian S, Ross JS, Stephens PJ, Miller VA, and Ali SM, et al (2015). Identification and characterization of RET fusions in advanced colorectal cancer. *Oncotarget* **6**, 28929–28937.

[32] Li FF, Yan P, Zhao ZX, Liu Z, Song DW, Zhao XW, Wang XS, Wang GY, and Liu SL (2016). Polymorphisms in the CHIT1 gene: associations with colorectal cancer. *Oncotarget* **7**, 39572–39581.

[33] Miao HK, Chen LP, Cai DP, Kong WJ, Xiao L, and Lin J (2015). MSH3 rs26279 polymorphism increases cancer risk: a meta-analysis. *Int J Clin Exp Pathol* **8**, 11060–11067.

[34] Leung ML, Davis A, Gao R, Casasent A, Wang Y, Sei E, Vilar E, Maru D, Kopetz S, and Navin NE (2017). Single-cell DNA sequencing reveals a late-dissemination model in metastatic colorectal cancer. *Genome Res* **27**, 1287–1299.

[35] Jin JP, Zhang Z, and Bautista JA (2008). Isoform diversity, regulation, and functional adaptation of troponin and calponin. *Crit Rev Eukaryot Gene Expr* **18**, 93–124.

[36] Liu R and Jin JP (2016). Calponin isoforms CNN1, CNN2 and CNN3: regulators for actin cytoskeleton functions in smooth muscle and non-muscle cells. *Gene* **585**, 143–153.

[37] Jayne D (2007). Molecular biology of peritoneal carcinomatosis. *Cancer Treat Res* **134**, 21–33.

[38] Daimon E, Shibukawa Y, and Wada Y (2013). Calponin 3 regulates stress fiber formation in dermal fibroblasts during wound healing. *Archives Dermatol Res* **305**, 571–584.

[39] Khawar IA, Kim JH, and Kuh HJ (2015). Improving drug delivery to solid tumors: priming the tumor microenvironment. *J Control Release* **201**, 78–89.

[40] Yilmaz M and Christofori G (2009). EMT, the cytoskeleton, and cancer cell invasion. *Cancer Metastasis Rev* **28**, 15–33.